Virology 528 (2019) 198–206

Contents lists available at ScienceDirect

Virology

journal homepage: www.elsevier.com/locate/virology

Viral replication centers and the DNA damage response in JC virus-infected cells

Kimberly D. Erickson[b], Robert L. Garcea[a,b,*]

[a] The Department of Molecular, Cellular, and Developmental Biology, University of Colorado, Boulder, CO 80309, United States
[b] The BioFrontiers Institute, University of Colorado, Boulder, CO 80309, United States

ARTICLE INFO

Keywords:
Polyomavirus
JCV
DNA damage response
Electron microscopy
Virus replication

ABSTRACT

JCV is a human polyomavirus (PyV) that establishes a persistent infection in its host. Current immunomodulatory therapies, such as Natalizumab for multiple sclerosis, can result in JCV reactivation, leading to the debilitating brain disease progressive multifocal leukoencephalopathy (PML). JCV is among the viruses that recruit and modulate the host DNA damage response (DDR) to replicate its genome. We have identified host proteins recruited to the nuclear sites of JC viral DNA (vDNA) replication using three cell types susceptible to infection *in vitro*. Using confocal microscopy, we found that JCV recruited a similar repertoire of host DDR proteins to these replication sites previously observed for other PyVs. Electron tomography of JCV "virus factories" showed structural features like those described for murine PyV. These results confirm and extend previous observations for PyVs to JCV emphasizing a similar replication strategy among members of this virus family.

1. Introduction

JC virus (JCV) is a human polyomavirus with a seroprevalence greater than 50% in studied populations (Kean et al., 2009b). Most primary infections are asymptomatic and occur by adolescence, with a gradual increase in incidence over subsequent years (Kean and Garcea, 2009a). JCV establishes a lifelong infection in the kidney and is frequently shed in the urine (Chesters et al., 1983; Dörries, 1984). Virus reactivation can occur in immunocompromised individuals, rarely resulting in progressive multifocal leukoencephalopathy (PML), a debilitating and often fatal infectious disease of the brain (Haley and Atwood, 2017). PML was prevalent during the AIDS epidemic because of immunosuppression from HIV infection but has subsequently decreased with improved retroviral management. However, new immunosuppressive regimens for the treatment of Crohn's disease and Multiple Sclerosis (MS) have increased the incidence of PML in these patient populations, in which prolonged immunosuppression allows reactivation and spread of JCV (Carson et al., 2009; Haley and Atwood, 2017; Kleinschmidt-DeMasters and Tyler, 2005; Langer-Gould et al., 2005; Van Assche et al., 2005; Zaheer and Berger, 2012). Unfortunately, the mechanisms of JCV reactivation and dissemination during immunosuppression are poorly understood.

Many DNA viruses affect cellular DNA repair mechanisms to enhance viral DNA replication (Carson et al., 2003; Evans and Hearing, 2005; Lilley et al., 2005; Wilkinson and Weller, 2004; Zhao et al., 2008). For polyomaviruses, (*e.g.,* BK virus (BKV), murine polyomavirus (MuPyV), and SV40), cellular DNA repair and cell cycle checkpoint proteins co-localize with sites of vDNA replication (Erickson et al., 2012; Heiser et al., 2016; Jiang et al., 2012; Verhalen et al., 2015; Zhao et al., 2008). These cellular proteins include those of the MRN complex (Mre11, Rad50, Nbs1), Chk2 kinase, γH2AX, and phosphorylated ATM (pATM). One possible reason for this colocalization is that viral replication intermediates, such as stalled replication forks, activate the cellular DNA damage response (DDR), and the induced cellular DNA repair proteins mitigate problematic structures arising from the rapid DNA replication of the viral genome (Heiser et al., 2016; Sowd et al., 2014, 2013). Viral proteins, such as polyomavirus small T-antigen, act to block cell cycle progression at the S-G2 boundary, in part through their interaction with the cell phosphatase PP2A, which allows sustained activation of critical checkpoint proteins (Bollag et al., 2010; Cicala et al., 1994; Pallas et al., 1990). By stalling cell cycle progression, the virus replicates in a prolonged S-phase, thereby increasing virus yields.

The specific sites of viral replication and assembly within the infected cell nucleus do not appear random, but are localized into distinct domains termed "virus assembly factories" (Erickson et al., 2012). These nuclear subdomains, where vDNA replication and packaging appear spatially coupled, likely represent a topology enabling rapid and

* Corresponding author at: The BioFrontiers Institute, University of Colorado, Boulder, CO 80309, United States.
E-mail address: garcear@colorado.edu (R.L. Garcea).

https://doi.org/10.1016/j.virol.2018.12.014
Received 19 November 2018; Received in revised form 19 December 2018; Accepted 19 December 2018
Available online 26 February 2019
0042-6822/

high-fidelity virion assembly. Nuclear assembly factories have been characterized during MuPyV infection of murine fibroblasts (Erickson et al., 2012), and at late times after infection, clusters of assembled virions within the nucleus are observed by electron microscopy (EM). Juxtaposed to these virion clusters are tubular structures composed of the major capsid protein VP1. The combination of tubular structures and virions has been termed a "virus factory," assuming that the tubular structures are assembly intermediates (Erickson et al., 2012; Mattern et al., 1967, 1966; Mattern and DeLeva, 1968). These structures have been resolved at high-resolution using electron tomography of infected cells, and a model has been proposed in which the tubular structures are part of an assembly platform for virion formation (Erickson et al., 2012). Importantly, similar tubular structures have been seen in electron micrographs of human PML brain biopsies, as well as cells transfected with plasmids encoding JCV capsid proteins, thus linking cell culture results with *in vivo* PML pathogenesis (Howatson et al., 1965; Mazlo and Tariska, 1980; Nagashima et al., 1982, 1981; Shishido-Hara et al., 2004, 2000; ZuRhein and Chou, 1965). Thus, these structures appear relevant to the *in vivo* replication and assembly of JCV in the human brain.

Studying JCV in cell culture has been problematic because of low infection efficiencies and the need to use chimeric viruses to enhance replication. We sought to validate and extend observations of JCV-infected transformed cell lines (SVG-A) by using primary cultures of astrocytes and choroid plexus (CP) cells. We found a similar repertoire of host proteins previously identified in other polyomavirus complexes localizing to sites of JCV vDNA replication. High-resolution tomographic reconstructions of JCV factories and immunogold staining demonstrate a close spatial relationship of DDR host proteins to these virus factories. Taken together, our data suggest strong similarities with MuPyV in the replication and assembly of JCV thus generalizing the "virus factory" model to JCV replication and virion assembly.

2. Materials and methods

2.1. Cell lines and virus strains

SVG-A cells (gift of Walter Atwood) are human fetal astrocytes transformed with a replication-defective SV40 (Major et al., 1985). SVG-A cells were grown in MEM (M2279, Sigma) supplemented with 10% fetal bovine serum (F0926, Sigma), streptomycin, penicillin, and beta-mercaptoethanol. Primary human astrocytes were purchased from ScienCell (1800) and grown in Astrocyte Medium (1801, ScienCell) on cell culture plates coated with poly-L-lysine (P1399, Sigma). Primary human choroid plexus cells were purchased from ScienCell (1310) and grown in epithelial Media (4101, ScienCell). All cells were maintained in a humidified environment at 37 °C with 5% CO_2. The virus strains, Mad1 and Mad4, were all generous gifts of Ellen Cahir-McFarland; the virus strain, Turbo, was a generous gift of Walter Atwood.

Cell culture infections were carried out in minimal volumes of virus diluted in cell culture media. Cells were incubated with virus at 37 °C for 2 hrs, media was added to cells and virus, and incubation continued at 37 °C with 5% CO_2 for the duration of the experiment. Cells were infected at a virus dilution that was pre-determined to give an infection efficiency of 40–60%, as determined by fluorescence-staining for Tag.

2.2. Antibodies

Antibodies for immunofluorescence studies were: T antigen (PAB2003, mouse, 1:250) (Bollag et al., 2000); VP1 (PAB597, mouse, 1:600, gift of Ellen Cahir-McFarland); pATM Ser1981 (05–740, Millipore, mouse, 1:1000); Nbs1 (NBS100-143, Novus, rabbit, 1:500); γ-H2AX (ab11174, AbCam, Rabbit, 1:1000); pCHK1 Ser345 (2348, Cell Signaling, rabbit, 1:500); pCHK1 Ser317 (12302, Cell Signaling, rabbit, 1:500); Rad51 (ab133534, AbCam, rabbit, 1:250); RPA32 (5F5, rat, 1:20, gift of H. Nasheuer); RPA70 (4D9, rat, 1:10, gift of H. Nasheuer); RPA14 (6119-B01P, AbNova, mouse, 1:50); pRPA32 Ser23 (8H3, rat, 1:5, gift of H. Nasheuer); pRPA32 Ser29 (8C7, rat, 1:2, gift of H. Nasheuer); pRPA32 Ser4/Ser8 (ab87277, AbCam, rabbit, 1:100). All secondary antibodies were AlexaFluor-conjugated (LifeTechnologies) and used at a 1:2000 dilution.

Antibodies directly-conjugated to fluorescent labels were: T-antigen (PAB2003, mouse, 1:250) conjugated to AlexaFluor-647; RPA32 (5F5, rat, 1:10) was conjugated to AlexaFluor-488; RPA70 (4D9, rat, 1:5) was conjugated to either AlexaFluor-488 or AlexaFluor-647. To conjugate fluorescent probes, antibodies were buffer exchanged into PBS by three passages through a 100 kDa spin column (Amicon Ultra, Millipore) and final resuspension in PBS to the original volume. Sodium bicarbonate (pH 9.0) was added to sample to 0.1 M final concentration followed by addition of the fluorescent moiety (resuspended in DMSO). The sample was incubated in the dark, with end-over-end mixing, at room temperature for 1 h. After incubation, the labeled antibody was buffer exchanged into PBS as described above.

For immunoelectron microscopy studies, antibodies were: anti-VP1 (PAB597, mouse, 1:100; 70 nm sections); pATM Ser1981 (05-740, Millipore, mouse, 1:50; 45 nm sections); Nbs1 (NBS100-143, Novus, rabbit, 1:200; 70 nm sections). Secondary antibodies were conjugated to 10 nm gold (Ted Pella Inc., Redding, CA) and diluted 1:20. All antibodies were diluted in 1% powdered nonfat milk reconstituted in phosphate-buffered saline (PBS) containing 0.02% Tween 20 (PBST).

2.3. Immunofluorescence

Cells were grown on acid-etched, poly-L-lysine-coated coverslips and infected with JCV as described above. Cells were prepared for immunofluorescence staining as previously described (Heiser et al., 2016; Zhao et al., 2008). Briefly, cells were washed three times with cold PBS solution followed by cytoskeleton buffer (CSK) [10 mM piperazine-N,N-bis(2-ethanesulfonic acid) (PIPES), pH 6.8, 100 mM NaCl, 300 mM sucrose, 1 mM $MgCl_2$, 1 mM EGTA]. Soluble proteins were pre-extracted for 3 mins with cold CSK containing 0.5% Triton X-100 and protease inhibitors (Complete mini tablets, Pierce) at 4 °C. The cells were then washed with PBS, fixed in 4% paraformaldehyde (PFA) in PBS for 20 min, washed with PBS, and blocked with 10% FBS / PBS at 4 °C. Samples were incubated with primary antibodies for 1 h at 37 °C, washed with PBS, and incubated with secondary antibodies for 1 h at 22 °C. Stained cells were mounted onto glass slides with ProLong anti-fade reagent containing Dapi (P36962, Invitrogen) and allowed to incubate at 22 °C overnight.

2.4. Fluorescence in situ Hybridization

JCV viral genomes were detected with nick-translated DNA probes specific for PyV DNA. Briefly, the entire JCV viral genome (SVE196, gift of W. Atwood) was cloned into pUC18 at *Bam*HI (pUC-JCV), and 2 μg plasmid DNA was labeled with ATTO550 using the PromoFluor Nick Translation Kit (PK-PF550-NTLK-10, Promokine), according to the manufacturer protocol. Labeled DNA was purified on PCR clean-up column (28106, Qiagen).

FISH analysis was performed as described previously (Heiser et al., 2016), with some modifications. Briefly, cells grown on coverslips were infected, fixed and immunostained for viral or host proteins, as described above. Immunostained cells were fixed a second time with 4% PFA in PBS to crosslink bound antibodies followed by treatment with 0.2 mg/ml RNase Type III (R5125, Sigma) in 2X SSC at 37ºC for 15 min and washed in 2X SSC 3 times. The JCV DNA probe was diluted in cDenHyb (D002, Insitus) and hybridized to samples for 3 mins at 90 °C then 2 mins each at 80ºC, 70ºC, 60ºC, 50ºC, and 45ºC followed by overnight incubation at 37ºC. Coverslips were washed at 45 °C with 1.5X SSC, 50% formamide/1.5X SSC, and 1.5X SSC for 5 mins each. Stained cells were mounted onto glass slides with ProLong anti-fade reagent containing Dapi (P36962, Invitrogen) and allowed to incubate

at 22 °C overnight.

2.5. EdU label and click-iT chemistry

EdU was added to media at a final concentration of 10 μM 1 h before fixation. Cells were incubated for 1 h at 37 °C in the presence of EdU; coverslips were washed once in PBS and immediately fixed and stained, as described above. The fluorescent dye conjugation reaction was performed according to manufacturer's protocol (C10637, Invitrogen) after antibody and FISH incubations.

2.6. Confocal microscopy

Confocal images were acquired on the Nikon A1R laser scanning confocal microscope, using a 1.45NA 100x objective and 405, 488, 561 and 638 laser lines. Image processing and analysis were completed using ImageJ analysis software (NIH). Data are shown as an extracted slice from the Z-stacks, unless otherwise noted.

2.7. High-pressure freezing

Infected cells were trypsinized and collected by centrifugation. The cell pellet was resuspended in growth media supplemented with either 20% dextran (40,210 Da, Sigma–Aldrich). The cell suspension (3 μl) was deposited into an aluminum planchette (Engineering Office M. Wohlwend GmbH, Sennwald, Switzerland) with a sample depth of 100 μm and vitrified in the Wohlwend Compact 02 high-pressure freezer under a pressure of 2000 bar by a jet of liquid nitrogen applied

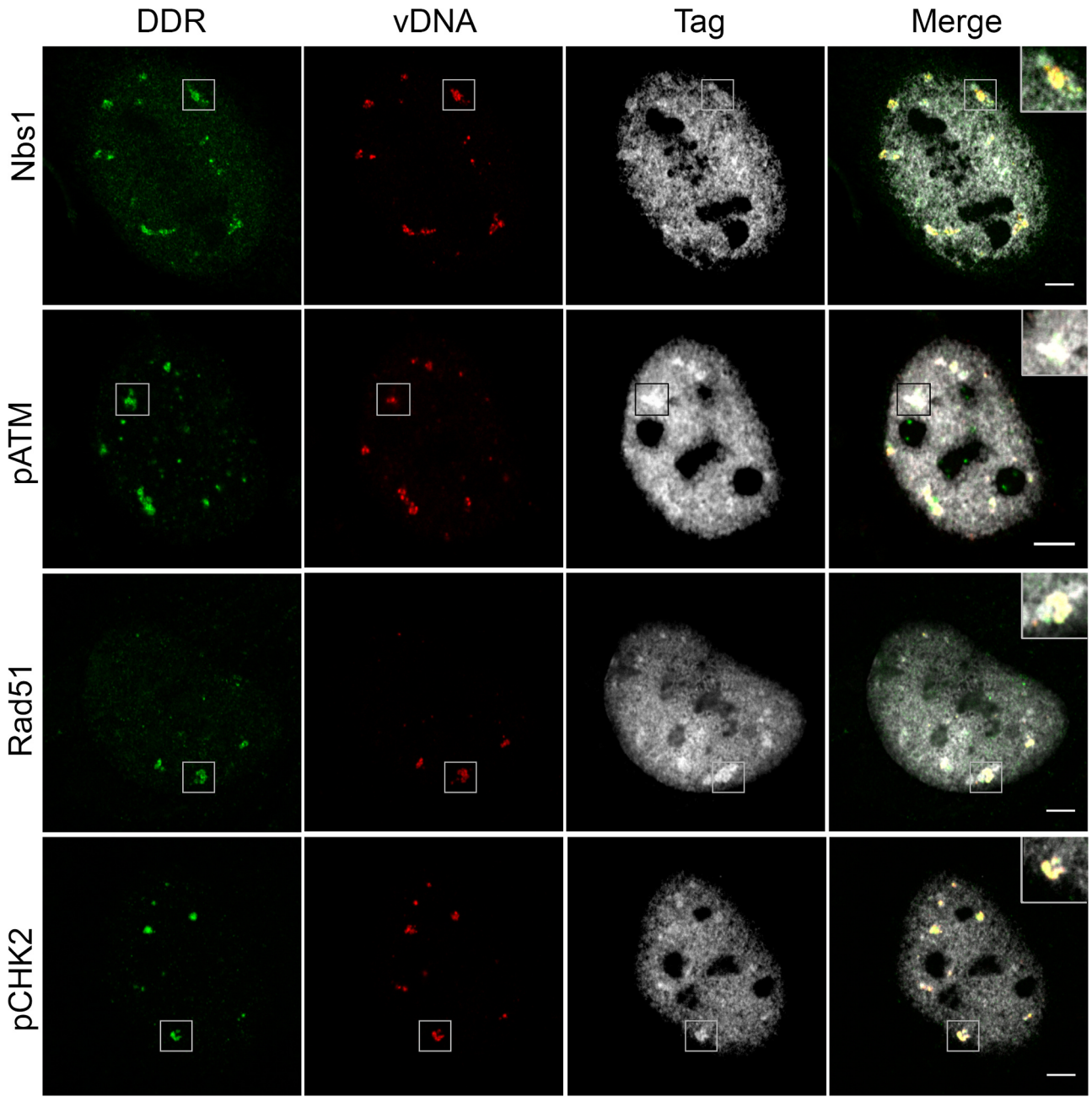

Fig. 1. Cellular DNA damage repair proteins localize to viral replication centers. Primary choroid plexus (CP) epithelial cells were infected with the Mad1 strain of JCV for 6 days. Cells were fixed and stained for the DDR protein (indicated to left of image) and Tag, followed by staining for vDNA using FISH. Stained cells were imaged on a Nikon A1R laser scanning confocal microscope. Images represent one slice of a Z-stack. "Merge" indicates merged images of each channel. Inset image is indicated by the gray box shown on each image and is zoomed in to show a representative viral replication center. Scale bar = 5 μm.

on the carrier. The frozen cell suspensions were stored in liquid nitrogen prior to cryo-substitution and plastic embedding.

2.8. Cryo-substitution

High-pressure frozen cells were cryo-substituted with 1% osmium tetroxide / 0.2% uranyl acetate in acetone over 3 days at −90 °C with gradual warming to room temperature over a period of 2 days. Samples were removed from planchettes and rinsed with acetone several times to remove residual osmium and uranyl acetate. Cells were infiltrated with increasing concentrations of Epon-Araldite 802 epoxy resin (Electron Microscopy Sciences, Port Washington, PA) over a period of 2 days, with three final incubations of 100% Epon to remove residual acetone. Samples were polymerized in BEEM™ embedding capsules (Electron Microscopy Sciences) by addition of DMP-30 accelerator and incubation at 60 °C for 2 days.

Samples used for immunogold-labeling, high-pressure frozen cells were cryosubstituted with 0.1% uranyl acetate / 0.25% glutaraldehyde in acetone at −75 °C for 3 days with gradual warming to −35 °C over 12 hrs. Cells were removed from the planchettes and rinsed with −35 °C acetone. Samples were infiltrated over 3 days with increasing concentrations of Lowicryl/HM20 resin (Electron Microscopy Sciences) mixed in acetone, with three final changes of 100% HM20. Resin-infiltrated cells were polymerized in BEEM capsules at −35 °C under ultraviolet light for 2 days. Samples and resin were maintained at −35 °C during infiltration steps in an automated freezing system (AFS; Leica Microsystems).

2.9. Electron microscopy

Epon-embedded sections were cut to a thickness of 70 nm with an UltraCut–UCT microtome (Leica Microsystems) using a diamond knife (Diatome, Biel, Switzerland). Sections were picked up on Formvar-coated copper slot grids and stained with 2% aqueous uranyl acetate for 10 mins, followed by Reynold's lead citrate (Reynolds, 1963) for 4 mins. Images were obtained on a Philips CM10 electron microscope operating at 80 kV.

2.10. Electron tomography

Semi-thick Epon-embedded sections (~300 nm) were stained with 2% uranyl acetate as described above for thin Epon-embedded sections. Colloidal gold particles (15 nm; BBI Research, Inc., Madison, WI) were placed on both grid surfaces to serve as fiducial markers for subsequent image alignment. Sections were imaged on an FEI Tecnai F20 microscope (FEI Company Ltd., Eindhoven, The Netherlands) operating at 200 kV and images were collected on a 4K by 4K CCD Ultrascan camera (Gatan, Inc., Pleasanton, CA). Dual-axis tilt series data sets were acquired using the SerialEM software package (Mastronarde, 2005). 1x1 images were acquired on serial sections; tomographic reconstructions

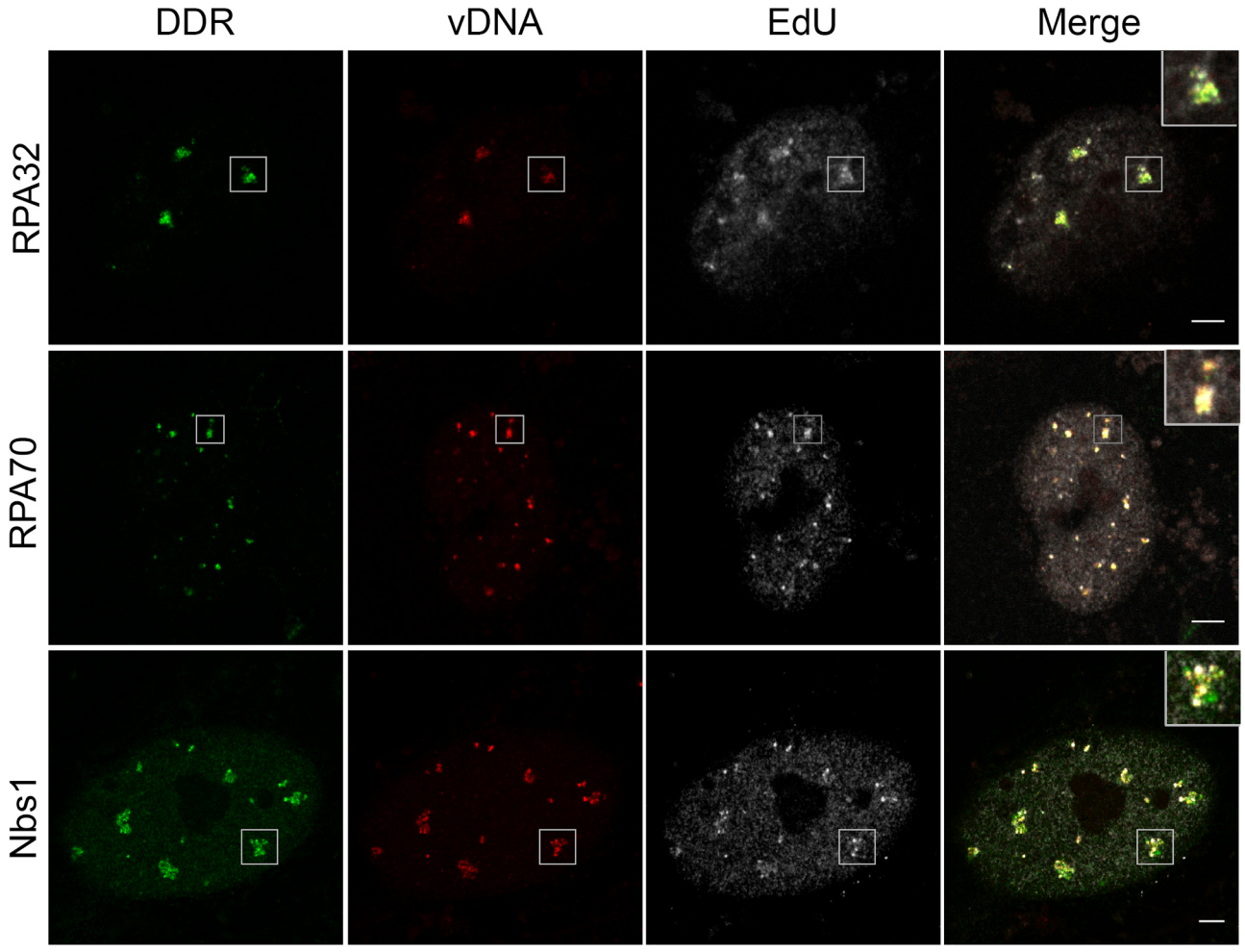

Fig. 2. The cellular RPA complex localizes to replicating vDNA. Primary CP cells were infected as described in Fig. 1 and pulsed with EdU for 1 h before fixation and staining for indicated DDR protein and vDNA (FISH). The EdU was detected following FISH with an azide-functionalized AlexaFluor 647 fluorescent molecule. Images represent one slice of a Z-stack. "Merge" indicates merged images of each channel. Inset image is indicated by the gray box shown on each image and is zoomed in to show a representative viral replication center. Scale bar = 5 μm.

and section alignments were produced by the IMOD software package (Kremer et al., 1996). 3D structures of interest were surface rendered using tools available in the IMOD software package (Mastronarde, 1997; Mastronarde and Held, 2017).

2.11. Immunogold electron microscopy

For immunogold labeling, Lowicryl-embedded samples were sectioned at a thickness of 45 nm (anti-pATM, anti-NBS1, anti-Tag) or 70 nm (anti-VP1) and picked up on Formvar-coated, nickel slot grids. Sections were fixed with 0.5% paraformaldehyde (diluted from a fresh stock (32%, Electron Microscopy Sciences) in PBS) for 15 min at 22 °C. The grids were rinsed with PBS and blocked in 1% powdered nonfat milk reconstituted in PBST in a humidified chamber for 30 min at room temperature followed by incubation in the same chamber on droplets of primary antibody diluted in 1% powdered nonfat milk reconstituted in PBST for 2 hrs at 22 °C. The grids were washed in a stream of PBS, blotted to remove excess PBS and incubated with gold-conjugated secondary antibody for 1 h at 22 °C. Samples were washed in a stream of PBS followed by a distilled water wash, air-dried and post-stained as described above except incubation times were reduced to 4 and 2 mins for methanolic uranyl acetate and lead citrate, respectively. Samples were imaged as described above.

3. Results

3.1. JCV recruits DNA damage response proteins

Polyomaviruses recruit host DNA damage response (DDR) proteins to sites of vDNA replication (Heiser et al., 2016; Sowd et al., 2013; Zhao et al., 2008). In MuPyV, SV40 and BKV-infected cells, DDR proteins such as pATM, the MRN complex, and ɣH2AX localize to sites of vDNA replication along with the viral protein, large T antigen (LTag) (Heiser et al., 2016; Jiang et al., 2012; Zhao et al., 2008). We used confocal microscopy to localize similar candidate proteins during replication of JCV. We tested three cell types: 1) primary human astrocytes, 2) SVG-A cells (SV40-transformed astrocytes (Major et al., 1985)), and 3) primary human choroid plexus (CP) epithelial cells. In addition, three virus strains of JCV were used: 1) Mad1, a prototype type I JCV strain isolated from the brain tissue of a patient with PML (Martin et al., 1985; Padgett et al., 1971), 2) Mad4, developed after multiple passages of Mad1 in cell culture (Martin et al., 1985; Padgett et al., 1977), and 3) Turbo (also called M1-SVEΔ), an engineered chimeric Mad1 genome with SV40 regulatory sequences (Vacante et al., 1989). We found DDR proteins localized at sites of vDNA replication regardless of the cell type or virus strain used (Fig. 1, Fig. S1). We proceeded to study both CP and astrocyte cells for DDR recruitment to viral replication centers in a non-transformed cell background.

Viral replication centers were identified using both anti-Tag antibodies and fluorescent *in situ* hybridization (FISH) using a JCV-specific DNA probe. We found that Nbs1, phospho-ATM, Rad51 and pCHK2 localized to sites of vDNA replication in infected cells (Fig. 1, Fig. S1). Phospho-CHK1 (pCHK1) did not localize to these sites in any cell type (data not shown). Of interest was the replication protein A (RPA) complex, a heterotrimer complex of three subunits, RPA70, RPA32 and RPA14 that binds to single-stranded DNA (ssDNA) during both normal cellular DNA replication and the response to DNA damage. RPA32 binds LTag of SV40, BKV, and JCV to aid in the resolution of replicating genomes (Fanning et al., 2006; Jiang et al., 2012; Orba et al., 2010). To determine whether the vDNA observed by FISH (Fig. 1) was replicating and bound by RPA, we used ClickiT EdU chemistry to detect replicating genomes. JCV-infected cells were pulsed with EdU before fixation and subsequent antibody staining. We found that the fluorescent signals for vDNA and EdU co-localized, indicating the vDNA was actively replicating at the time of the EdU pulse (Fig. 2). All three RPA proteins (RPA70, 32 and 14) along with other DDR proteins localized to these sites of replicating viral genomes (Fig. 2, Fig. S2), consistent with results previously seen for MuPyV, and with reports of SV40 replication and MuPyV Tag binding to RPA (Arunkumar et al., 2005; Banerjee et al., 2013). These results suggest that JCV exploits components of the DDR pathway in a similar manner in different cell types studied. The list of host proteins examined using confocal microscopy is summarized in Table 1.

Table 1
List of DDR proteins examined by confocal microscopy during JCV infection.

Host Protein	Role in DNA damage repair/ replication	Colocalize with vDNA
ɣ-H2A.x	Histone mark of DNA damage	Yes
pATM	Kinase signals MRN complex to dsDNA break	Yes
Mre11	MRN complex; Initiate dsDNA break	N/A[a]
Rad50	repair process	N/A[a]
Nbs1		Yes
pChk1	Cell cycle kinase	No
pChk2		Yes
RPA70	Replication Protein A (RPA) complex;	Yes
RPA32	Binds ssDNA	Yes[b]
RPA14		Yes
Rad51	Displaces RPA on ssDNA; assists in DNA repair	Yes
TopoI	Cleave and relax dsDNA; help promote	No
TopoIIβ	proper supercoiling of dsDNA	Yes

[a] All antibodies tested did not work for IF analysis.
[b] Includes antibodies that recognize phosphorylated RPA32 (pRPA32).

3.2. JCV replication during infection of primary astrocytes

Astrocytes may support JCV infection *in vivo* (Mazlo and Tariska, 1982) and we investigated the virus life cycle of primary astrocyte cells in culture. Previously, it was found that astrocytes replicate JCV poorly and do not produce detectable levels of progeny virions (our data not shown; (Mazlo and Tariska, 1982)). We observed two populations of viral replication centers in primary astrocyte cells by immunofluorescence (Fig. 3A and B). In one population, EdU, vDNA, and Tag were co-localized (Fig. 3A, EdU = vDNA = Tag), while in the second population, vDNA and Tag co-localized but without EdU-labeled DNA (Fig. 3B, EdU ≠ vDNA = Tag). In these latter cell nuclei, the EdU signal was localized at areas separate from vDNA and Tag, likely at sites of cellular DNA synthesis. These data suggest the second population of cells replicated vDNA but had ceased active replication at the time of EdU labeling. When primary astrocytes were stained for RPA32 or other DDR proteins (pATM, Nbs1), instead of Tag, we observed a similar staining pattern described above for Tag, where vDNA and DDR proteins were colocalized but did not colocalize with EdU label (EdU ≠ vDNA = DDR; Fig. S3). These results suggest that both viral and cellular components of the replication centers remained with replicated vDNA in the absence of active replication.

3.3. Immunoelectron microscopy of JCV-infected SVG-A cells

By electron microscopy (EM), vDNA replication and virion assembly have been localized to distinct regions in MuPyV-infected cell nuclei, and we have termed these areas consisting of virions and tubular structures as “virus factories” (Erickson et al., 2012). However, viral replication centers (*e.g.,* sites of vDNA replication) remain undefined using EM techniques. Similar to EM visualization of MuPyV-infected mouse fibroblasts, we observed unstructured, electron-dense regions adjacent to the virus factories in JCV-infected SVG-A cells. These regions appeared only in infected nuclei and were distinct from heterochromatin (Erickson et al., 2012). To determine if these regions might represent viral replication centers, we used immunogold electron microscopy (IEM) of thin-sections of JCV-infected SVG-A cells labeled

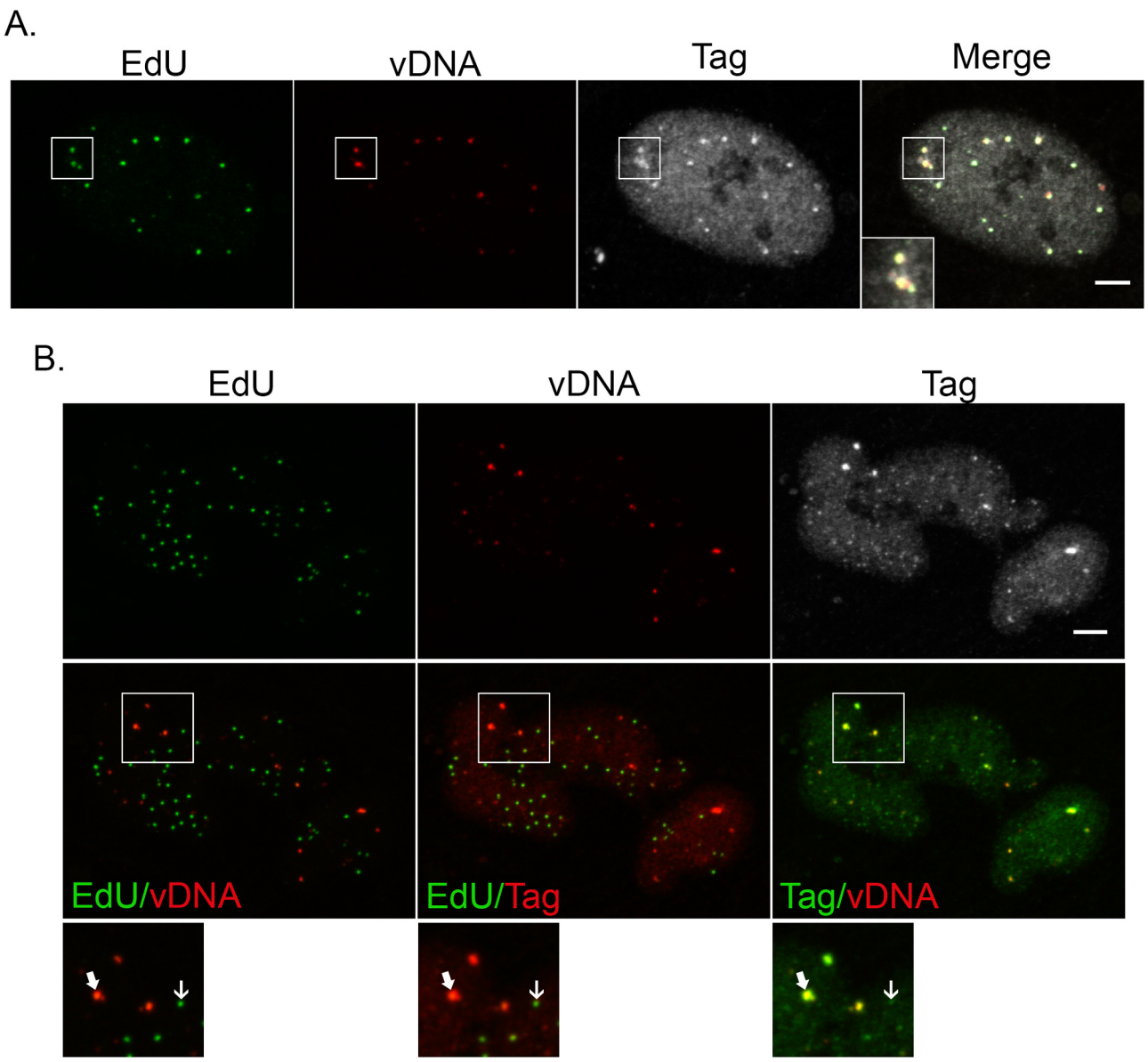

Fig. 3. Viral replication in primary human astrocytes reveals two populations of infected cells. Primary astrocytes were infected and pulsed with EdU as described in Fig. 2. Images represent the max projection of a Z-stack. Merged images were pseudo-colored to highlight regions of co-localization; the colored text indicates the channel signal. Scale bar = 5 μm. A) Mad1-infected astrocytes replicating JCV where the EdU signal colocalizes with both the vDNA and Tag signals (EdU = vDNA = Tag); B) Mad1-infected astrocytes during infection where the EdU signal does not colocalize with vDNA and Tag signals (EdU ≠ vDNA = Tag); cell is from same population of cells shown in (A). The region in the white box is enlarged below each merged image to highlight fluorescent signals; thick arrow, indicates either vDNA or Tag (or merged signals in the final panel); arrow, indicates EdU signal.

with antibodies to DDR proteins. IEM allowed localization of proteins (*e.g.,* DDR) in proximity to sites of virion accumulation. Nbs1 and pATM staining was localized adjacent to progeny virions at electron dense regions within the nucleus (Fig. 4A, B). As a control, VP1 staining was localized to progeny virions and not the electron dense regions (Fig. 4C). The Tag antibody was incompatible with the preparation of samples for IEM, possibly due to loss of antigenicity during sample processing. Localization of Nbs1 and pATM adjacent to virions was consistent with the model that virus assembly occurs adjacent to areas of vDNA replication.

3.4. Electron microscopy of JC virus factories

Tubular structures observed as part of MuPyV factories may represent an assembly intermediate and previously have been defined using high-resolution electron tomography of MuPyV-infected cells (Erickson et al., 2012). Electron micrographs of PML brain biopsies also show progeny virions associated with tubular structures (Mazlo and Tariska, 1980; Nagashima et al., 1982, 1981; Silverman and Rubinstein, 1965). To obtain high-resolution images of JCV "factories," we infected SVG-A cells with either the Turbo or Mad4 virus strains and processed the cells by high-pressure freezing and freeze-substitution.

Infected cells were identified in thin sections (70 nm) and subsequent thick serial sections (300 nm) of cells were prepared, tomograms collected and modeled using IMOD software (Kremer et al., 1996; Mastronarde, 1997; Mastronarde and Held, 2017). We observed that the "tubes" observed for MuPyV (Erickson et al., 2012) and in PML brain pathologies (Mazlo and Tariska, 1980; Nagashima et al., 1982, 1981; Silverman and Rubinstein, 1965) were present in JCV-infected SVG-A cells (Fig. 5; Supplementary Movie 1 and 2). However, the tubular structures in Turbo-infected cells were smaller (30 nm; Supplementary Move 2) than those seen in either MuPyV-infected cells

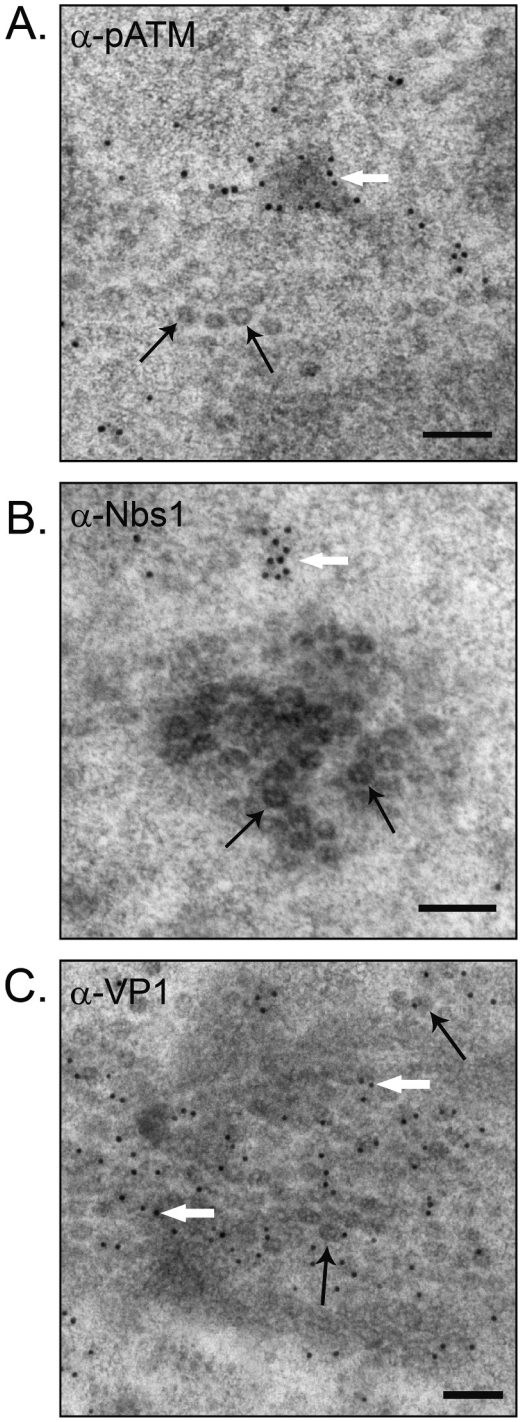

Fig. 4. DDR proteins localize adjacent to virus factories. Freeze-substituted thin sections (either 45 or 70 nm) of Mad4-infected SVG-A cells were incubated with indicated primary antibodies followed by secondary detection with 10 nm gold-conjugated secondary antibodies. A) anti-phosphoATM (45 nm); B) anti-Nbs1 (70 nm); or C) anti-VP1 (70 nm). Stained sections were imaged on a FEI Tecnai T12 electron microscope operating at 100 kV. White arrows, immunogold staining; black arrows, virions; scale bars represent 100 nm.

(Erickson et al., 2012) or SVG-A cells infected with MAD4 (45 nm; Fig. 5) or CP cells infected with MAD1 (45 nm; Fig. S4). Also, progeny virions appeared to "bud" from the side of the tubes, as well as from the ends of the tubes, as previously observed for MuPyV (Erickson et al., 2012) (Fig. 5B).

Supplementary material related to this article can be found online at doi:10.1016/j.virol.2018.12.014.

4. Discussion

These results further define sites of JCV DNA replication during infection of primary human cells and identified a repertoire of host proteins that localize to viral replication centers. Given that many of these proteins have been identified during infection by other polyomaviruses (SV40, BKV, MuPyV), and between different cell types during JCV-infection, it is likely that the various polyomaviruses recruit DDR proteins to facilitate genome replication. High-resolution electron tomograms of virus factories (Fig. 5) revealed that JCV forms tubular structures, like MuPyV, and immunoelectron microscopy showed that DDR proteins localized near these virus factories. Together, these results support the model that vDNA replication and virus assembly are spatially-coupled.

Our data support and extend previous observations of DDR protein localization in JCV-infected cells (Orba et al., 2010). Previous experiments localized DDR proteins in a neuroblastoma cell line, IMR-32, where the authors argue that JCV-infection induces a G2 arrest in this cell line. Similar to our findings, this study shows the same DDR proteins, except for pCHK1, localize to sites of vDNA replication. While we did not observe relocalization of pCHK1 in any JCV-infected cell examined (despite the antibody recognizing pCHK1 in UV-irradiated cells), this result could be due to differences in the genetic background of the cells. IMR-32 cells were isolated from a metastatic abdominal mass and is a mix of neuroblastoma-like cells and fibroblasts (Tumilowicz et al., 1970). Thus, cells transformed *in vivo* may exhibit altered signaling pathways from either primary cells or glial cells transformed *in vitro*. Furthermore, we extended our light microscopy observations to high-resolution virus structures and localized DDR proteins relative to virus factories.

Polyomavirus-infected cells enter S-phase to replicate vDNA efficiently; however, the kinetics of infection in cell culture differs widely between polyomaviruses. The SVG-A cell line and Turbo strain of JCV were developed to improve viral replication in cell culture (Major et al., 1985; Vacante et al., 1989), and therefore their infection may not represent physiological JCV replication. Therefore, we evaluated the replication and assembly of JCV in non-transformed, but physiologically-relevant, primary astrocyte and choroid plexus cells. In MuPyV-infected fibroblasts, virus replication centers are visible by confocal microscopy within 18 h after infection (Erickson et al., 2012; Heiser et al., 2016). However, in JCV-infected cells replication centers did not appear until five to six days post-infection (Figs. 1 and 2), consistent with qPCR data (not shown) and previous studies of the kinetics of JCV infection (Frisque et al., 1979; Padgett et al., 1977). The cell types described and used in the current study showed some differences with respect to vDNA replication and virus production. The immunofluorescence data suggest that infected astrocytes may either pause or stop vDNA replication and resume cellular DNA replication. One possibility is that astrocytes cannot continue replicating vDNA and abort the infection process altogether. A second possibility is that astrocytes pause vDNA replication and then re-initiate vDNA replication at a later time. The replication characteristics we observed in astrocytes may represent one of many different infection outcomes that may occur in different types of neuronal cells. Infection of CP epithelia may represent an alternate route of JCV infection in the brain. JCV infection of CP epithelia was reported for a patient who succumbed to JCV-associated meningitis (Agnihotri et al., 2014). Our cell culture data suggest that CP epithelia can be infected and produce virus, consistent with recent studies (Agnihotri et al., 2014; O'Hara et al., 2018). Thus, the CP could be a site of infection in the brain facilitating PML or other JCV-related encephalopathies. While we understand that using primary cell culture is not the same as *in vivo* studies, the genetic background of primary cells is more analogous to *in vivo* conditions. Thus, by using different cell culture systems, we could develop a more complete understanding of JCV infection.

Immunoelectron microscopy provided evidence for the spatial

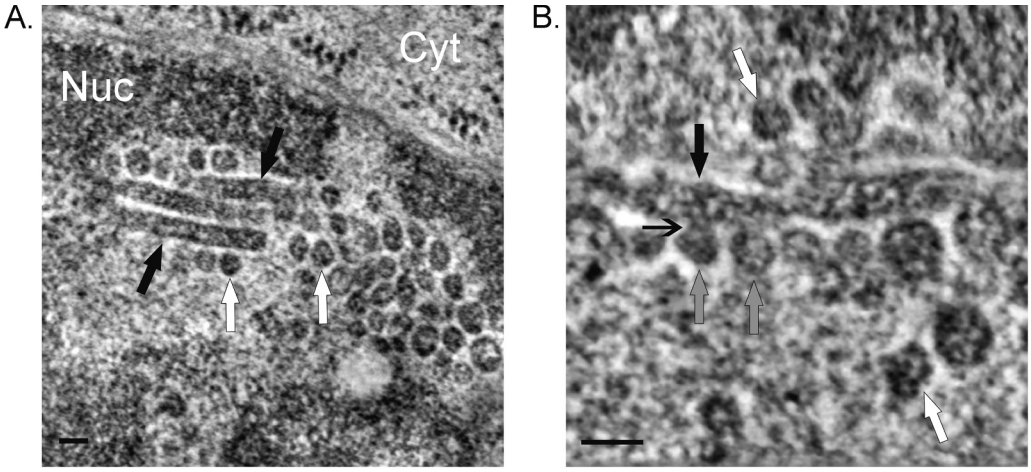

Fig. 5. Electron tomography of JCV-infected cells reveals tubular assembly intermediates. Images from dual-axis tomograms of high pressure frozen, freeze-substituted, and Epon-embedded, 300 nm thick sections Mad4-infected SVG-A cells. A) Image represents a 25 nm *in silico* slice from the tomogram; tubular structures (black arrow) are present in the periphery of the condensed chromatin adjacent to virions (white arrows); Nuc, nucleus; Cyt, cytoplasm; x and y-rotational axes are set at 0°; B) A 5 nm *in silico* slice of the image shown in (A); the image was rotated around the x-axis -37.1° to illustrate the virions budding from the side of the tube; black arrow, tubular structure; white arrow, virions not associated with a tube; gray arrow, tube-associated virions; black arrowhead, attachment of virion to tube; Scale bar = 50 nm (A, B). A movie of the full tomograms for each cell and the model can be found as Supplementary Movies S1 (Mad4) and S2 (Turbo).

positioning of DDR proteins with virus factories. We found that antibodies stained electron dense regions adjacent to progeny virions. We hypothesize the dense regions may be viral replication centers, as these dense regions were not observed in uninfected nuclei. These observations suggest that virus genome replication occurs in distinct, but adjacent areas to virus assembly, suggesting the two processes may be spatially coupled.

Electron tomography of JCV-infected cells (Fig. 5, Supplementary movies S1 and S2) revealed tubular structures similar to those observed both in MuPyV-infected cells (Erickson et al., 2012) and brain biopsies from PML patients (Nagashima et al., 1982, 1981; Silverman and Rubinstein, 1965). We postulate that these tubular structures, which are comprised of VP1, are possible assembly intermediates, with virions budding from the tubes. Unlike MuPyV, where virions bud from the ends of the tubular structures (Erickson et al., 2012), we found virions budding from the side of the JCV tubes (Fig. 5). This difference could reflect the slower kinetics of JCV replication and assembly (days *versus* hrs) or an alternate assembly strategy. We did not observe virus factories in primary astrocytes by EM, consistent with these cells supporting early vDNA replication but not progressing to productive infection (Mazlo and Tariska, 1982).

It is unclear why we observed the smaller tube diameter in tomographic reconstructions of SVG-A cells infected with Turbo. It is possible that genetic differences between the virus strains results in smaller tubes, since SVG-A cells infected with Mad4 virus strain exhibit tube diameters similar to MuPyV tubes (~40–45 nm). Turbo has an insertion of SV40 sequence within the JCV origin to yield more efficient replication in cell culture. This insertion is close to the late promoter and thus may affect either the expression or processing of the late proteins (agnoprotein, VP1, VP2 and VP3) (Vacante et al., 1989) and changes in the late (but not early) transcripts of Turbo compared to Mad1 have been noted previously (Vacante et al., 1989).

Our studies, in combination with previous reports, provide details of the JCV life cycle, particularly regarding JCV infection in the brain. We have extended observations from other polyomaviruses to JCV-infected cells to develop a “virus factory” model of JCV replication and virion assembly. Based on the data presented here, we propose polyomaviruses use similar mechanisms for vDNA replication by recruiting DDR proteins. However, the cell background or *in vivo* conditions can influence the transition from vDNA replication to progeny virus formation. Additionally, while JCV and MuPyV tubular intermediates are structurally similar, the mechanism of virus budding from the tubes may differ between viruses. Taken together, these data can assist in identifying potential new therapeutic targets that can help resolve JCV-associated brain pathologies that result from immune suppression.

JCV infection is problematic for individuals undergoing immunosuppressive therapies. MS patients treated with natalizumab are at risk for developing PML due to reactivation of JCV in the brain. The host proteins identified in our study are potential therapeutic targets for JCV-infected individuals with reactivated virus replication. Small molecule inhibitors of DNA damage proteins and inhibitors of the ATM/ATR pathways have been tested in clinical trials as therapeutic targets in tumors (Weber and Ryan, 2015). Potentially, these inhibitors could interfere with JCV reactivation by inhibiting the pATM that relocalizes to sites of virus replication. By studying the life cycle of JCV in different cell types in culture, we provide a more comprehensive model of JCV replication and assembly, which can be used to identify targets of future anti-JCV therapies.

Acknowledgements

The authors would like to thank Walter Atwood for the SVG-A cell line and Turbo virus strain, Ellen Cahir-McFarland for Mad1 and Mad4 virus strains and antibodies to JCV proteins, and Heinz Nasheuer for the RPA antibodies. We are grateful to the BioFrontiers Advanced Light Microscopy Core Facility and its director, Joe Dragavon, for instrument use and helpful advice; CU Boulder Electron Microscope Core Facility and its director, Garry Morgan, for instrument use. We would like to thank Eileen O’Toole and Janet Fox for their guidance and expertise with electron tomography and the IMOD software. Finally, we thank members of the Garcea laboratory, past and present, for their continued support.

This work was funded by NIH/NCI grant R01 CA37667 and a grant from the PML Consortium.

Appendix A. Supporting information

Supplementary data associated with this article can be found in the online version at doi:10.1016/j.virol.2018.12.014.

References

Agnihotri, S.P., Wuthrich, C., Dang, X., Nauen, D., Karimi, R., Viscidi, R., Bord, E., Batson, S., Troncoso, J., Koralnik, I.J., 2014. A fatal case of JC virus meningitis presenting with hydrocephalus in a human immunodeficiency virus-seronegative patient. Ann. Neurol. 76, 140–147.

Arunkumar, A.I., Klimovich, V., Jiang, X., Ott, R.D., Mizoue, L., Fanning, E., Chazin, W.J., 2005. Insights into hRPA32 C-terminal domain-mediated assembly of the simian virus 40 replisome. Nat. Struct. Mol. Biol. 12, 332–339.

Banerjee, P., DeJesus, R., Gjoerup, O.V., Schaffhausen, B.S., 2013. Viral interference with DNA repair by targeting of the single-stranded DNA binding protein RPA. PLoS Pathog. 9, 1–11.

Bollag, B., Hofstetter, C.A., Reviriego-Mendoza, M.M., Frisque, R.J., 2010. JC virus small t

antigen binds phosphatase PP2A and Rb family proteins and is required for efficient viral DNA replication activity. PLoS One 5, 1–12.
Bollag, B., Prins, C., Snyder, E.L., Frisque, R.J., 2000. Purified JC virus T and T' proteins differentially interact with the retinoblastoma family of tumor suppressor proteins. Virology 274, 165–178.
Carson, C.T., Schwartz, R.A., Stracker, T.H., Lilley, C.E., Lee, D.V., Weitzman, M.D., 2003. The Mre11 complex is required for ATM activation and the G2/M checkpoint. EMBO J. 22, 6610–6620.
Carson, K., Focosi, D., Major, E.O., Petrini, M., Richey, E., West, D., Bennett, C., 2009. Monoclonal antibody-associated progressive multifocal leucoencephalopathy in patients treated with rituximab, natalizumab, and efalizumab: a review from the Research on Adverse Drug Events and Reports (RADAR) Project. Lancet Oncol. 10, 816–824.
Chesters, P.M., Heritage, J., McCance, D.J., 1983. Persistence of DNA sequences of BK virus and JC virus in normal human tissues and in diseased tissues. J. Infect. Dis. 147, 676–684.
Cicala, C., Avantaggiati, M.L., Graessmann, A., Rundell, K., Levine, A.S., Carbone, M., 1994. Simian virus 40 small-t antigen stimulates viral DNA replication in permissive monkey cells. J. Virol. 68, 3138–3144.
Dörries, K., 1984. Progressive multifocal leucoencephalopathy: Analysis of JC virus DNA from brain and kidney tissue. Virus Res. 1, 25–38.
Erickson, K.D., Bouchet-Marquis, C., Heiser, K., Szomolanyi-Tsuda, E., Mishra, R., Lamothe, B., Hoenger, A., Garcea, R.L., 2012. Virion assembly factories in the nucleus of polyomavirus-infected cells. PLoS Pathog. 8, 1–15.
Evans, J.D., Hearing, P., 2005. Relocalization of the Mre11-Rad50-Nbs1 complex by the adenovirus E4 ORF3 protein is required for viral replication. J. Virol. 79, 6207–6215.
Fanning, E., Klimovich, V., Nager, A.R., 2006. A dynamic model for replication protein A (RPA) function in DNA processing pathways. Nucleic Acids Res 34, 4126–4137.
Frisque, R.J., Martin, J.D., Padgett, B.L., Walker, D.L., 1979. Infectivity of the DNA from four isolates of JC virus. J. Virol. 32, 476–482.
Haley, S.A., Atwood, W.J., 2017. Progressive multifocal leukoencephalopathy: endemic viruses and lethal brain disease. Annu. Rev. Virol 4, 349–367.
Heiser, K., Nicholas, C., Garcea, R.L., 2016. Activation of DNA damage repair pathways by murine polyomavirus. Virology 497, 346–356.
Howatson, A.F., Nagai, M., ZuRhein, G.M., 1965. Polyoma-like virions in a human demyelinating disease. Acta Neuropathol. 93, 379–386.
Jiang, M., Zhao, L., Gamez, M., Imperiale, M.J., 2012. Roles of ATM and ATR-mediated DNA damage responses during lytic BK polyomavirus infection. PLoS Pathog. 8, 1–12.
Kean, J.M., Garcea, R.L., 2009a. Polyomaviruses and Disease, in: Damania, B., Pipas, J.M. (Eds.), DNA Tumor Viruses. pp. 53–74.
Kean, J.M., Rao, S., Wang, M., Garcea, R.L., 2009b. Seroepidemiology of human polyomaviruses. PLoS Pathog. 5, 1–10.
Kleinschmidt-DeMasters, B., Tyler, K., 2005. Progressive multifocal leukoencephalopathy complicating treatment with natalizumab and interferon beta-1a for multiple sclerosis. N. Engl. J. Med. 353, 369–374.
Kremer, J.R., Mastronarde, D., McIntosh, J.R., 1996. Computer visualization of three-dimensional image data using IMOD. J. Struct. Biol. 116, 71–76.
Langer-Gould, A., Atlas, S., Green, A., Bollen, A., Pelletier, D., 2005. Progressive multifocal leukoencephalophathy in a patient treated with natalizumab. N. Engl. J. Med. 353, 375–381.
Lilley, C.E., Carson, C.T., Muotri, A.R., Gage, F.H., Weitzman, M.D., 2005. DNA repair proteins affect the lifecycle of herpes simplex virus 1. Proc. Natl. Acad. Sci. U. S. A. 102, 5844–5849.
Major, E.O., Miller, A.E., Mourrain, P., Traub, R.G., de Widt, E., Sever, J., 1985. Establishment of a line of human fetal glial cells that supports JC virus multiplication. Proc. Natl. Acad. Sci. U. S. A. 82, 1257–1261.
Martin, J.D., King, D.M., Slauch, J.M., Frisque, R.J., 1985. Differences in regulatory sequences of naturally occurring JC virus variants. J. Virol. 53, 306–311.
Mastronarde, D., 2005. Automated electron microscope tomography using robust prediction of specimen movements. J. Struct. Biol. 152, 36–51.
Mastronarde, D., 1997. Dual-axis tomography: An approach with alignment methods that preserve resolution. J. Struct. Biol. 120, 343–352.
Mastronarde, D., Held, S.R., 2017. Automated tilt series alignment and tomographic reconstruction in IMOD. J. Struct. Biol. 197, 102–113.
Mattern, C.F., DeLeva, A.M., 1968. Observations on polyoma virus filaments Virology.
Mattern, C.F., Takemoto, K.K., Daniel, W.A., 1966. Replication of polyoma virus in mouse embryo cells: Electron microscopic observations. Virology 30, 242–256.
Mattern, C.F., Takemoto, K.K., DeLeva, A.M., 1967. Electron microscopic observations on multiple polyoma virus-related particles. Virology 32, 378–392.
Mazlo, M., Tariska, I., 1982. Are astrocytes infected in progressive multifocal leukoencephalopathy (PML)? Acta Neuropathol. 56, 45–51.
Mazlo, M., Tariska, I., 1980. Morphological demonstration of the first phase of polyomavirus replication in oligodendroglia cells of human brain in progressive multifocal leukoencephalopathy (PML). Acta Neuropathol. 49, 133–143.
Nagashima, K., Yamaguchi, K., Nakase, H., Miyazaki, J., 1982. Progressive multifocal leukoencephalopathy: A case report and review of the literature. Acta Pathol. Japan 32, 333–343.
Nagashima, K., Yamaguchi, K., Yasui, K., Ogiwara, H., 1981. Progressive multifocal leukoencephalopathy: neuropathology and virus isolation. Acta Pathol. Japan 31, 953–961.
O'Hara, B.A., Gee, G.V., Atwood, W.J., Haley, S.A., 2018. Susceptibility of primary human choroid plexus epithelial cells and meningeal cells to infection by JC virus. J. Virol. 92, e00105–e00118.
Orba, Y., Suzuki, T., Makino, Y., Kubota, K., Tanaka, S., Kimura, T., Sawa, H., 2010. Large T antigen promotes JC virus replication in G2-arrested cells by inducing ATM- and ATR-mediated G2 checkpoint signaling. J. Biol. Chem. 285, 1544–1554.
Padgett, B.L., Rogers, C.M., Walker, D.L., 1977. JC virus, a human polyomavirus associated with progressive multifocal leukoencephalopathy: additional biological characteristics and antigenic relationships. Infect Immun 15, 656–662.
Padgett, B.L., Walker, D.L., ZuRhein, G.M., Eckroade, R.J., Dessel, B.H., 1971. Cultivation of papova-like virus from human brain with progressive multifocal leucoencephalopathy. Lancet (London, England) 1, 1257–1260.
Pallas, D.C., Shahrik, L.K., Martin, B.L., Jaspers, S., Miller, T.B., Brautigan, D.L., Roberts, T.M., 1990. Polyoma small and middle T antigens and SV40 small t antigen form stable complexes with protein phosphatase 2A. Cell 60, 167–176.
Reynolds, E.S., 1963. The use of lead citrate stain at high pH in electron microscopy. J. Cell Biol. 17, 208–212.
Shishido-Hara, Y., Hara, Y., Larson, T., Yasui, K., Nagashima, K., Stoner, G.L., 2000. Analysis of capsid formation of human polyomavirus JC (Tokyo-1 strain) by a eukaryotic expression system: splicing of late RNAs, translation and nuclear transport of major capsid protein VP1, and capsid assembly. J. Virol. 74, 1840–1853.
Shishido-Hara, Y., Ichinose, S., Higuchi, K., Hara, Y., Yasui, K., 2004. Major and minor capsid proteins of human polyomavirus JC cooperatively accumulate to nuclear domain 10 for assembly into virions. J. Virol. 78, 9890–9903.
Silverman, L., Rubinstein, L.J., 1965. Electron microscopic observations on a case of progressive multifocal leukoencephalopathy. Acta Neuropathol. 5, 215–224.
Sowd, G.A., Li, N.Y., Fanning, E., 2013. ATM and ATR activities maintain replication fork integrity during SV40 chromatin replication. PLoS Pathog. 9, 1–15.
Sowd, G.A., Mody, D., Eggold, J., Cortez, D., Friedman, K.L., Fanning, E., 2014. SV40 Utilizes ATM kinase activity to prevent non-homologous end joining of broken viral DNA replication products. PLoS Pathog. 10, 1–20.
Tumilowicz, J.J., Nichols, W.W., Cholon, J.J., Greene, A.E., 1970. Definition of a continuous human cell line derived from neuroblastoma. Cancer Res. 30, 2110–2118.
Vacante, D.A., Traub, R., Major, E.O., 1989. Extension of JC virus host range to monkey cells by insertion of a simian virus 40 enhancer into the JC virus regulatory region. Virology 170, 353–361.
Van Assche, G., Van Ranst, M., Sciot, R., Dubois, B., Vermeire, S., Noman, M., Verbeeck, J., Geboes, K., Robberecht, W., Rutgeerts, P., 2005. Progressive multifocal leukoencephalopathy after natalizumab therapy for Crohn's disease. N. Engl. J. Med. 353, 362–368.
Verhalen, B., Justice, J.L., Imperiale, M.J., Jiang, M., 2015. Viral DNA replication-dependent DNA damage response activation during BK polyomavirus infection. J. Virol. 89, 5032–5039.
Weber, A.M., Ryan, A.J., 2015. ATM and ATR as therapeutic targets in cancer. Pharmacol. Ther. 149, 124–138.
Wilkinson, D.E., Weller, S.K., 2004. Recruitment of cellular recombination and repair proteins to sites of herpes simplex virus type 1 DNA replication is dependent on the composition of viral proteins within prereplicative sites and correlates with the induction of the DNA damage response. J. Virol. 78, 4783–4796.
Zaheer, F., Berger, J., 2012. Treatment-related progressive multifocal leukoencephalopathy: current understanding and future steps. Ther Adv Drug Saf 3, 227–239.
Zhao, X., Madden-Fuentes, R.J., Lou, B.X., Pipas, J.M., Gerhardt, J., Rigell, C.J., Fanning, E., 2008. Ataxia telangiectasia-mutated damage-signaling kinase- and proteasome-dependent destruction of Mre11-Rad50-Nbs1 subunits in Simian virus 40-infected primate cells. J Virol 82, 5316–5328.
ZuRhein, G.M., Chou, S.-M., 1965. Particles resembling papova viruses in human cerebral demyelinating disease. Science 80 (148), 1477–1479.